Jiang *et al. Cancer Nanotechnology* (2022) 13:19
https://doi.org/10.1186/s12645-022-00125-y

Cancer Nanotechnology

RESEARCH Open Access

Small tumour microparticle enhances drug delivery efficiency and therapeutic antitumour efficacy

Zhou Jiang[1], Kai Li[2], Yongzhong Luo[1], Bin Chen[2], Fanfan Meng[2], Huifang Yi[1], Lemeng Zhang[1], Hua Yang[1], Wenwei Zhou[1], Tianli Cheng[1], Huihuang Yi[1], Qing Yi[1], Xiaoping Wen[1], Sheng Hu[4], Hongyan Liu[3*] and Jianhua Chen[1*]

*Correspondence: hongyanliu03@126.com; Cjh_1000@163.com

[1] Department of Thoracic Medicine, Affiliated Cancer Hospital of Xiangya School of Medicine, Central South University, Hunan Cancer Hospital, 410006 Changsha, China
[2] Hubei Engineering Research Center of Tumour-Targeted Biochemotherapy, 430030 Wuhan, China
[3] Respiratory and Critical Care Medicine, Second Affiliated Hospital of Anhui Medical University, 230601 Hefei, China
[4] Department of Thoracic Oncology, Tongji Medical College, Hubei Cancer Hospital, Huazhong University of Science and Technology, Wuhan, China

Abstract

Background: Targeted delivery of chemotherapeutic drugs to tumour cells is a major challenge for cancer chemotherapy. Recent studies show that tumour cell-derived microparticles can be used as vectors to package chemotherapeutic drugs, and selectively deliver drugs to tumour cells. Nevertheless, since the particle size range of microparticles is relatively wide, the sizes may exhibit different pharmacokinetic characteristics in the body, which will have a great impact on the application of drug-loaded microparticles. Here in this report, we compare the characteristics, distribution in vivo and antitumour efficacy of small microparticles (SMPs, $\leq$ 200 nm) and large microparticles (LMPs, > 200 nm) which loaded with methotrexate, in order to screen out more suitable carrier sizes.

Results: In vivo and in vitro studies have proved that the drug-loaded vesicles of SMPs (mainly 100–200 nm) are more reasonable, and the drug content and maintenance in tumour tissues. The time is significantly higher than that of LMPs (mainly 400–500 nm). At the same time, we found that SMPs can be better taken up and processed by DC cells to promote the proliferation of specific T cells. SMPs show obvious advantages in both drug delivery and immune activation, which is verified by the comparison of the efficacy of SMPs and LMPs in the treatment of solid tumours in mice.

Conclusions: The present data demonstrate that the SMPs had a higher cumulative concentration in tumour tissue, and the tumour suppressive effect was also significantly better than that of LMPs. It provides important process parameters for the drug-loaded vesicle delivery system. Future works will aim to expand production scale and improve the separation and purification process of the microparticles. Although the research and application of drug-loaded vesicles derived from tumour cells is still in its infancy, it has broad prospects for tumour therapy.

Keywords: Drug-loaded microparticles, Distribution metabolism, Activation of DC cells, Antitumour immunity

Background

Microparticles (MPs), also known as microvesicles (MVs), are small vesicle-like structures that generated by a regulated outward budding from the plasma membrane during eukaryotic cell apoptosis or activation (Mathieu et al. 2019). MPs are between 100 and 1000 nm diameters in size, serve as carriers for the exchange of substances between cells, mediate cell–cell communication, and participate in various physiological and pathological processes (Mause and Weber 2010; Yuana Yuana et al. 2013). Tumour cell-derived MPs (TMPs) can be used as carriers to deliver chemotherapeutic drugs and specifically activate anti-tumour immune response (Tang et al. 2012; Liang et al. 2019; Zhang et al. 2015; Khani et al. 2021). Compared with synthetic nano-drug carriers, chemotherapeutic TMPs have high affinity for tumour cells, excellent biocompatibility and low side effects. Therefore, they have a broader application prospect in tumour immunotherapy (Guo et al. 2019; Gao et al. 2020).

The particle size of drug carrier has an important influence on its pharmacokinetics in vivo, is a key parameter of enhanced permeability and retention (EPR) effect. Nanoparticles must evade clearance by the reticuloendothelial system (RES). The RES mainly distributes in the liver and spleen and plays a critical role in removing particles and soluble substances from the circulation and tissues. Nanoparticles of 30–150 nm are located in bone marrow (Moghimi and Moghimi 1995), whereas particles of 150–300 nm are found mainly in the liver and the spleen (Moghimi and Moghimi 1995). Depending on the reports, the "ideal" size requirements for nanoparticles developed for cancer treatment are between 70 and 200 nm (Storm et al. 1995). Therefore, a well-designed drug carrier should follow the design principles of biological barriers for nano-drug delivery (Blanco et al. 2015). In this study, in order to maximally avoid the elimination of RES and make better use of EPR effect, we sorted the TMPs into two size ranges by hierarchical filtration, relatively small TMPs ($\leq$ 200 nm) and relatively large TMPs (> 200 nm). Further, we compared the characteristics, distribution and anti-tumour efficacy of two different sizes methotrexate-loaded TMPs (MTX-TMPs). It was confirmed that small MTX-TMPs had a higher cumulative concentration in tumour tissue, and the tumour suppressive effect was also significantly better than that of large MTX-TMPs.

Results

Preparation and characterization of MTX-TMPs of different sizes

In this study, MTX was incorporated into TMPs by incubation with human A549 cells (lung cancer) at 37 ℃ under a period of ultraviolet (UVB, 300 J m^{-2}) irradiation. MTX-TMPs were extracted according to conventional differential centrifugation (Guo et al. 2019). The MTX-TMPs precipitate resuspension was filtered through a membrane filter of 1 μm pore size to ensure that their particle size was less than 1 μm (Fig. 1A). Nanoparticle size is a decisive factor for distribution, and 200 nm is an important size demarcation point. Therefore, small microparticles (SMPs, $\leq$ 200 nm) and large microparticles (LMPs, > 200 nm) were separated by size-exclusion chromatography. Nanoparticle tracking analysis (NTA) revealed that SMPs had diameters ranging from 50 to 480 nm, with a mean diameter of 179 nm and a peak (mode) diameter of ~ 145 nm, whereas LMPs ranged from 330 to 800 nm, with a mean diameter of 462 nm and a peak (mode) diameter

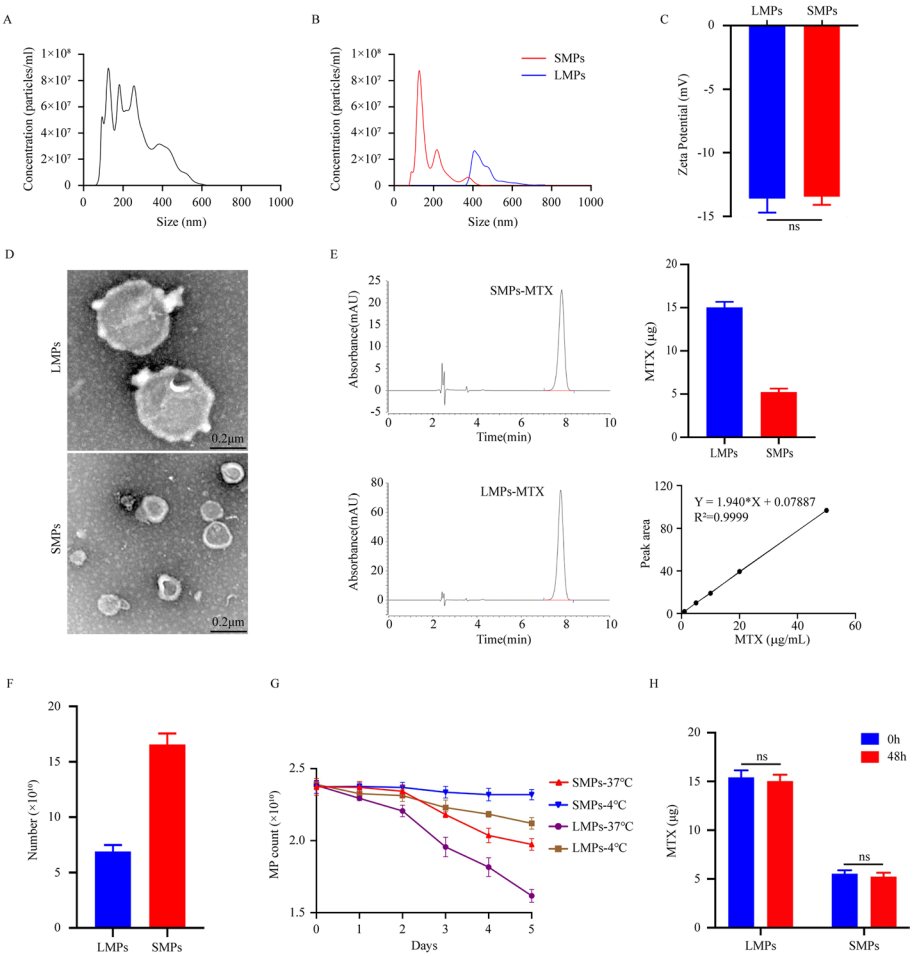

Fig. 1 Preparation and characterization of different sizes of MTX-TMPs. **A** A549 cells (1×10^8) were exposed to a concentration gradient of MTX (1 mg/ml) under UV irradiation for the preparation of MTX-TMPs. MTX-TMPs were isolated by gradient centrifugation, and the concentration and particle size was analysed by nanoparticle tracking analysis (NTA). **B** Small microparticles (SMPs) and large microparticles (LMPs) were separated by size-exclusion chromatography. The size distribution was analysed by NTA. **C** Zeta potential of SMPs and LMPs, as measured by Dynamic light scattering (DLS). Data are presented as means ± s.d. ($n = 3$). **D** Morphology of SMPs and LMPs were analysed by transmission electron microscope. Scale bars, 200 nm. **E** The calibration curves showed good linearity over the concentration ranges of 1–50 μg/ml for MTX, $Y = 1.940^*X + 0.07887$, $R^2 = 0.9999$. The concentration of MTX loaded in 1×10^{10} SMPs and LMPs was measured by HPLC. **F** The radio of the number of SMPs and LMPs containing 10 μg MTX (n = 3). **G** Verification of the storage stability of two groups of MTX-TMPs. The same number of SMPs and LMPs were stored at 4 and 37 °C, respectively, and the corresponding number was detected from Day 0 to Day 5 ($n = 3$). **H** SMPs and LMPs were stored at 4 °C, and the stability of the loaded MTX was detected by HPLC at 48 h ($n = 3$)

of 410 nm (Fig. 1B). The TMPs were monodisperse and irregularly spherical, as observed by the transmission electron microscopy (TEM, and the sizes of SMPs and LMPs were basically the same as those determined by NTA (Fig. 1D). The Zeta potentials of two sizes MTX-TMPs were measured and there were no significant differences (Fig. 1C). Further high-performance liquid chromatography (HPLC) analysis showed that the MTX content was approximately 15 μg in per unit LMPs (about 1×10^{10} TMPs per unit), which was three times that of MTX in SMPs (Fig. 1E). This means that the number of SMPs was about 3 times that of LMPs in order to achieve the same drug dose (Fig. 1F). To confirm the preservation stability of MTX-TMPs, SMPs and LMPs were, respectively,

stored in normal saline at 4 and 37 °C, the quantity was measured within 5 days. The results showed that the number of SMPs remained unchanged in 5 days at 4 °C, but the number of SMPs was reduced by 1/5 on the fifth day at 37 °C. The quantity of LMPs had dropped by 10% at 4℃ and 30% at 37℃ on the fifth day. It could be observed that SMPs had better stability than LMPs (Fig. 1G). However, there was no significant difference in the number of TMPs and MTX content between SMPs and LMPs within 48 h at 4℃ (Fig. 1H). The following experiments were done using TMPs with equal MTX content prepared within 48 h.

Drug-packaging SMPs possess enhanced ability to accumulate in tumours

The ideal drug carrier size should be characterized by enhanced tumour accumulation and deep tumour penetration to efficiently reach tumour cells. Flow cytometry analysis was performed on the A549 cells incubated with membrane-bound fluorescent dye PKH26-labelled SMPs and LMPs for 0, 2, 4 and 6 h. The results showed a time-dependent uptake of TMPs by A549 cells, the SMP uptake rate was 65%, while LMPs was only 50% after incubation for 6 h (Fig. 2A). These results indicated that the TMPs with size less than 200 nm were more easily captured by A549 cells. But from the average fluorescence intensity, there was little difference between the two vesicles. It may be due to the larger volume of single PKH26-LMPs, so it had stronger fluorescence intensity (Fig. 2B, C). A similar phenomenon could also be observed with confocal laser scanning microscopy (CLSM), A549 cells uptook more red fluorescent SMPs in the same incubation time (Fig. 2D). Next, we studied the biodistribution of SMPs and LMPs in the subcutaneous tumour-bearing mice by labelling TMPs with near-infrared fluorescence dye 1,1′-dioctadecyl-3,3,3′,3′-tetramethylindotricarbocyanine iodide (DiR). DiR-labelled MPs were intravenously injected into mice on the 14th day after LLC inoculation. In the group that received DiR-LMPs, fluorescence was mainly distributed in the liver and spleen and secondarily in lung, kidney and tumour, whereas in DiR-SMPs, fluorescence was mainly distributed in the liver, spleen and tumour. The fluorescence intensity of tumour tissue in the DiR-SMPs group was significantly higher than that of DiR-LMPs, indicating that SMPs penetrated the tumour more easily, and still maintained a high level fluorescence in the tumour at the 24-h time point (Fig. 2E). Next, we investigated the MTX concentration in main organs and tumour. Tissue samples (heart, liver, spleen, lung, kidney, and tumour) were collected and analysed with HPLC. At 30 min after intravenous injection, MTX underwent rapid distribution to the main organs in each group (Fig. 2F). In bare MTX group, MTX easily diffused into other organs but less MTX accumulated in tumours. In groups of SMPs and LMPs, MTX concentration in tumours was significantly higher than that in bare MTX group at all time points, indicating encapsulation of MTX into SMPs and LMPs can achieve in vivo redistribution of MTX. We noted that SMPs and LMPs show relatively high concentration of MTX in liver and spleen at the 24-h time point. A previous study also reported that extracellular vesicles displayed a predominant localization in the liver and the spleen. The MTX of SMPs continued to accumulate in tumours within 24 h, while the MTX of LMPs gradually decreased at 8-h time point, and the concentration of MTX reduced by exactly one half (50%) compared with the highest amount at 2-h time point (Fig. 2F). Taken together, these results suggest

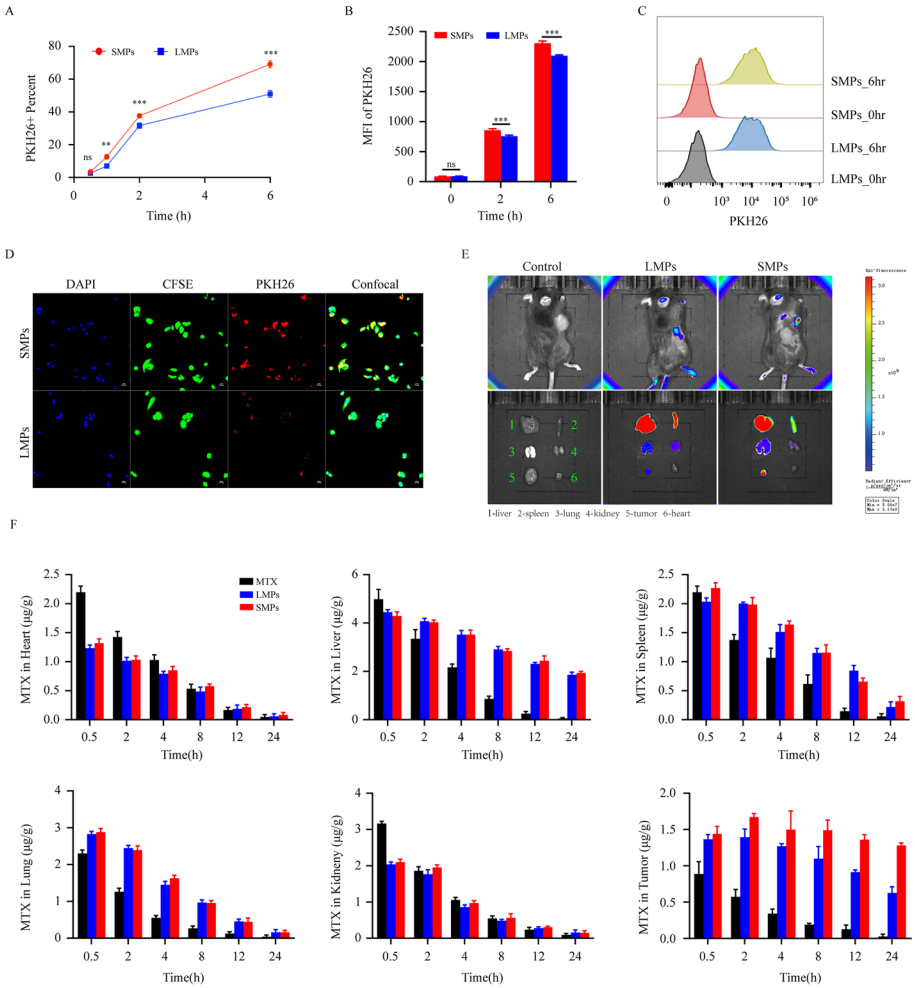

Fig. 2 Drug-loaded SMPs have an enhanced ability to accumulate in tumours. **A**–**C** Uptake of PKH26-stained MPs by A549 cells at different times. PKH26-stained MPs were incubated with A549 cells, the cell uptake ratio and average fluorescence intensity were detected by flow cytometry at different times. **A** PKH26 positive ratio. **B**, **C** Mean fluorescence intensity (MFI) of PKH26. **D** Confocal fluorescence showed the subcellular localization of PKH26-MPs uptake by A549 cells. PKH26-stained MPs were incubated with CFSE-stained A549 cells, after 20 h, cells were stained with DAPI and observed under two-photon laser scanning fluorescence microscope. Scale bar = 20 μm. **E** In vivo distribution of MPs. Lewis cells were subcutaneously inoculated into C57 mice on Day 0, and DiR-labelled MPs were intravenously injected into the mice on Day 14, and fluorescence imaging of live and isolated organs was performed 24 h later. The organs in the left column were liver, lung and tumour from top to bottom, and the organs in the right column were spleen, kidney and heart from top to bottom. **F** Detection of drug loading in organs. Mice with Lewis subcutaneous tumours were injected intravenously with methotrexate-loaded MPs, and their organs and tissues were taken at different times, and the amount of methotrexate in each organ tissue was detected by high-performance liquid chromatography ($n = 3$)

that SMPs possess enhanced ability to mediate MTX extravasation and penetration into tumour tissues than that of LMPs.

Antitumour activity of intravenously administered MTX-TMPs in murine tumour-bearing models

To investigate the potential effect of MTX-TMPs on tumours in mice, SMPs (10 μg, 2×10^{10} particles) or LMPs (10 μg, 0.67×10^{10} particles) were intravenously injected into

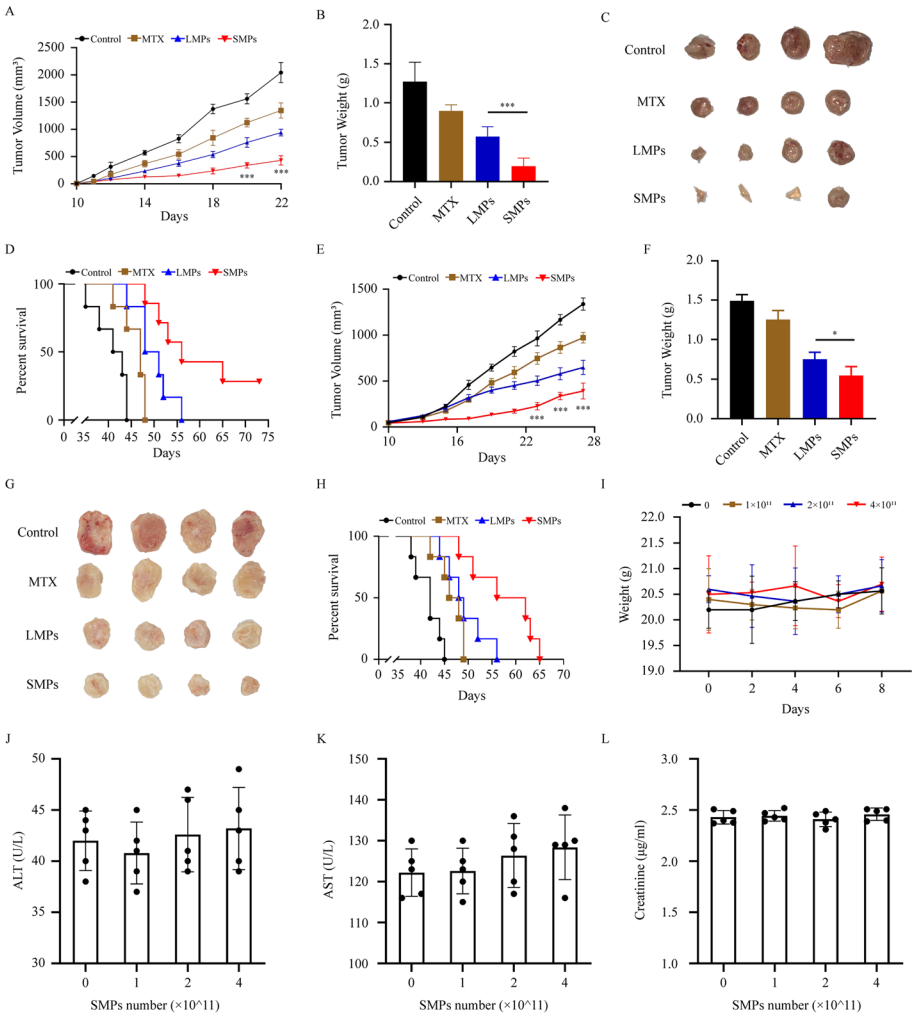

Fig. 3 Tumour treatment with MTX-MPs in vivo. **A**–**D** Methotrexate-loaded MPs in the treatment of LLC subcutaneous tumour model. C57 mice were inoculated with 1×10^5 Lewis cells subcutaneously on Day 0. On Day 7, 10 μg SMPs and 10 μg LMPs were injected intravenously, once every other day, for a total of 6 times, and the tumour volume was measured every other day. 6 mice were dissected and the tumour weights were measured on Day 22, and the survival period of the remaining 6 mice was counted. **A** The volume and **B** the weight of the mice subcutaneous tumour. **C** Pictures of tumours after MPs treatment. **D** Survival curve of mice ($n = 6$). **E**–**H** Methotrexate-loaded MPs in the treatment of A549 subcutaneous tumour model. BALB/c Nude mice were inoculated with 5×10^5 A549 cells subcutaneously on Day 0. On Day 7, 10 μg SMPs and 10 μg LMPs were injected intravenously, once every other day, for a total of 6 times, and the tumour volume was measured every other day. 6 mice were dissected and the tumour weights were measured on Day 20, and the survival period of the remaining 6 mice was counted. **E** The volume and **F** the weight of the mice subcutaneous tumour. **G** Pictures of tumours after MPs treatment. **H** Survival curve of mice ($n = 6$). Statistical analysis was performed by Student's t-test in Graphpad Prism 8 software (Graphpad Software Inc., USA), $n = 6$ in each group, and the values were reported as mean ± standard error of mean (SEM), $^*p < 0.05$, $^{**}p < 0.01$, $^{***}p < 0.005$, $^{****}p < 0.001$. **I**–**L** In vivo safety of SMPs.Healthy BALB/c mice were injected intravenously with SMPs, once every other day, 4 times in total. Blood was collected 48 h after the last injection to detect the biochemical indicators of the mice. **I** Body weight of mice. **J** Alanine transaminase (ALT). **K** Aspartate aminotransferase (AST). **L** Creatinine. $N = 5$ in each group, and the values were reported as mean ± SEM

C57BL/6 mice bearing ~ 50 mm^3 LLC tumours, once every other day, 6 times in total. Compared with NS, MTX 10 μg, treatment with LMPs significantly halted the development and progression of the tumour mass (Fig. 3A, B). However, SMPs exhibited the

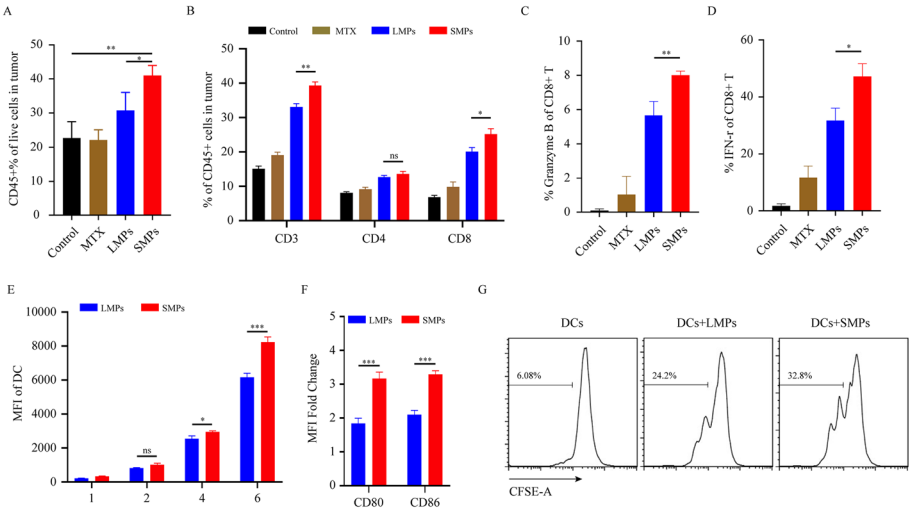

Fig. 4 Infiltrating immune cell proportion alternation in pleural tumour after LMPs and SMPs treatment. **A**–**C** Methotrexate-loaded LMPs and SMPs in the treatment of LLC subcutaneous tumour model, immune cell infiltration in the tumour (**A**), the proportion of T cells in immune cells (**B**), the expression of granzyme B (**C**) and IFN- γ (**D**) in killer T cells. **E**–**G** Activation of dendritic cells by LMPs and SMPs. PKH26-stained LMPs and SMPs were incubated with bone marrow-derived DCs (BALB/c background), the average fluorescence intensity were detected by flow cytometry at different times (**E**), multiple of expression of dendritic cell surface molecules CD80 and CD86 after co-incubation for 24 h (**F**), percentage of proliferating cells after incubation of CFSE-stained dendritic cells with MPs (**G**). Student's t-test was used for data statistics, $n = 3$ in each group. The value is the mean ± SEM, $^{*}P < 0.05$, $^{**}P < 0.01$, $^{***}P < 0.005$

strongest inhibitory effect, achieving 48.1% tumour shrinkage compared with LMPs. Life-span analysis showed that the median survival durations of NS, MTX, LMPs and SMPs 42, 47, 49.5, and 56 days, respectively. The survival time of SMPs group was significantly longer than that of the other three groups, and approximately 33% of the mice survived and the subcutaneous tumour disappeared after 65 days of SMPs treatment. The anti-tumour effect of SMPs was also proven in the A549 subcutaneous tumour model in nude mice, but the effect slightly worse than that in the LLC models (Fig. 3E–H). It has been reported that tumour microparticles stimulate dendritic cells via cGAS/STING signalling, and then activate specific anti-tumour T cells to kill tumours. Therefore, T cells may play a more important role in the process of MTX-TMPs killing tumours. A549 tumour-bearing BALB/c nude mice lacked thymus gland and had a repressed immune system due to reduced number of T cells. We inferred that tumour suppression decreased was due to the reduction of T cells leading to the failure of immune regulation function of SMPs. Notably, SMPs neither induced the hair and weight changes (Fig. 3I) nor altered liver and kidney functions (Fig. 3J–L). Together, these data suggest that methotrexate-loaded SMPs may generate a better treatment outcome against cancers and possess good security in vivo.

DC cells uptook more SMPs and induced tumour-specific $CD8^+$ T cells

To investigate the therapeutic potency of T-cell specific immune response, TILs in LLC tumours of C57BL/6 mice were isolated and analysed after 4 injections of TMPs.

As shown in Fig. 4A, $CD45^+$ cells increased in the two TMPs groups, especially in the SMPs group. Further analysis of the T cell subsets, compared with the control group and the MTX group, $CD3^+CD8^+$T cells in the SMPs group were more than doubled, and also significantly more than the LMPs group (Fig. 4B). The $CD8^+$ T cells of the SMPs group produced more Granzyme B and IFN-γ after being re-stimulated by PMA in vitro, indicating that these $CD8^+$ T cells had stronger anti-tumour activity (Fig. 4C, D). TMPs carry large amounts of tumour-associated antigens, which were taken up and processed by DCs and presented on the surface of DCs. Bone marrow-derived immature DCs were incubated with PKH-26-labelled SMPs and LMPs for 2, 4, 8 h. We found that compared with DCs incubated with LMPs, DCs incubated with SMPs were detected higher fluorescence intensity (Fig. 4E). This result showed that DCs had a better uptake capacity for SMPs. From the phenotypic and functional properties of DCs, upregulation of CD80 and CD86 in SMPs treatment group demonstrated that it was more conducive to the activation of DCs (Fig. 4E). T cells were isolated from spleen of C57BL/6 mice by magnetic activated cell sorting (MACS) and stained with CFSE. Then, the DC cells treated with SMPs and LMPs were incubated with T cells, and the proliferation of T cells was detected 4 days later. DCs treated with SMPs can better promote the proliferation and activation of T cells (Fig. 4F). These data suggest that DCs are more likely to take up small-sized TMPs and induce more effective specific T cell immune responses.

Discussion

Chemotherapy is the most important method of clinical cancer therapy, but the therapeutic effect has been greatly limited due to its toxic side effects and the drug resistance of tumour cells. We need very effective means to target chemotherapeutic drugs in order to have enough chemotherapeutic drugs into tumour cells. With the development of materials science and synthetic chemistry, new nanomaterial technology has developed rapidly in recent years. Nanocarriers are synthesized with high-molecular polymers to load chemotherapeutic drugs, and selectively deliver drugs to tumour cells and increase drug concentration in tumour cells and reduce the killing action of chemotherapeutic drugs on normal cells. However, these synthetic nanoparticles often change the normal operating system of the body after entering the body, including the immune system, enzyme reaction system, redox system, etc., which makes it more difficult for nanotechnology to apply in clinical treatment.

Microparticles derived from cell membranes, the critical mediators of intercellular communication, have attracted widespread attention as a natural drug delivery system. Microparticles derived from tumour cells as a special type of extracellular vesicles are quite different from synthetic microparticles and possess multiple advantages in cancer treatment. (i) Targeting tumour cells: TMPs are derived from tumour cells, have histocompatibility with tumour cells, hardly taken up by normal tissue cells (Tang et al. 2012). (ii) Safety and absence of toxicity for the body, due to the low total drug load (Guo et al. 2019; Gao et al. 2020). (iii) Reversing the drug resistance of tumour cells: stem cell-like cancer cells (SCLCCs) are a subset of cancer cells that can self-renew, multiple drug resistance and are highly tumorigenic. SCLCCs can take up more drug-loaded TMPs due to their low cell stiffness, more likely to be killed by drug-loaded TMPs. In addition, drug-loaded TMPs can down-regulate the expression of multidrug resistance proteins in

SCLCCs, inhibit their efflux of chemotherapeutic drugs, and reverse tumour resistance (Ma et al. 2016). (iv) Mobilize various types of immune cells to kill tumour cells, reprogramme tumour immune microenvironment. MTX-TMPs can mobilize and activate neutrophils, which display an antitumour N1 phenotype (Xu et al. 2020). Interestingly, macrophages are commonly polarized to tumour-associated M2 macrophages by TMPs (Ruihua et al. 2016), while drug-loaded TMPs can switch M2 phenotype to proinflammatory M1 that can kill tumour cells (Yanling et al. 2017). Although the specific mechanism is not yet clear, drug-loaded TMPs has indeed promoted tremendous functional changes of macrophages, thereby reprogrammed the immune microenvironment.

Microparticles have distinctive characteristics that make them more suitable for use as drug delivery systems than synthetic lipid carriers. Nevertheless, more efforts are needed to realize the conversion application of microparticles. Obstacles that need to be overcome for clinical applications include scaling up the microparticles production and separation process, as well as guidelines for proper storage. In addition, more and more in-depth studies of microparticles biogenesis, classification, subgroups, and internalization and transportation pathways in recipient cells are essential for further understanding of strategies to further improve microparticles as drug carriers.

Conclusions

This study classified the drug-loaded vesicles according to the size of the drug-loaded vesicles. In vivo and in vitro studies have proved that the drug-loaded vesicles of SMPs (mainly 100–200 nm) are more reasonable, and the drug content and maintenance in tumour tissues. The time is significantly higher than that of LMPs (mainly 400–500 nm). At the same time, we found that SMPs can be better taken up and processed by DC cells to promote the proliferation of specific T cells. SMPs show obvious advantages in both drug delivery and immune activation, which is verified by the comparison of the efficacy of SMPs and LMPs in the treatment of solid tumors in mice. This research provides important process parameters for the drug-loaded vesicle delivery system. Although the research and application of drug-loaded vesicles derived from tumour cells is still in its infancy, it has broad prospects for tumour immunotherapy.

Methods

Animals and cell lines

C57BL/6 mice were purchased from Hubei Provincial Center for Disease Control and Prevention. BALB/c Nude mice were purchased from Beijing Vital River Laboratory Animal Technology Co., Ltd. The experimental mice weighed 16 to 18 g and were females between 6 and 8 weeks old. All mice were raised in Hubei Provincial Food and Drug Safety Evaluation Center, in a specific pathogen free (SPF) environment, with a 12 h light/12 h dark cycle, 21 ℃–25 ℃, 40–60% humidity.

All cell lines including mouse Lewis lung carcinoma (LLC) cell line and human lung cancer cell line A549 were purchased from the China Center for Type Culture Collection (Wuhan, China). All cell lines were adherent cells, cultured in a cell incubator under the condition of 37 °C and 5% CO_2, and passaged at a ratio of 1 in 3 every 2 days. LLC cells were cultured in Dulbecco's modified Eagle medium (DMEM) with 8% fetal bovine

serum (FBS), and A549 cells were maintained in RPMI1640 medium (Thermo Fisher Scientific) with 8% FBS.

Preparation and isolation of MTX-TMPs

2×10^8 tumour cells (LLC or A549 cells) were resuspended in 20 ml serum free DMEM or RPMI 1640, exposed to ultraviolet light (UVB, 300 J/m^2) for 60 min, and then methotrexate (MTX, molecular formula: C20H22N8O5) was added to a final concentration of 2 mg/ml. The cells were cultured for 20 h, and the supernatants were collected for centrifugation: first 10 min at 500×*g*, and then 2 min at 14,000×*g* to clear cell debris, finally, the supernatants were centrifuged for 60 min at 14,000×*g* to pellet MTX-TMPs. The pellets were washed and resuspended in 0.9% saline or PBS for subsequent experiments. MTX-TMPs were separated into SMPs and LMPs through the Izon qEV10-70 columns. Allowed MTX-TMPs with 10 ml of 0.9% saline to run into the column, added 70 ml 0.9% saline and collected the void-volume. The optimal fraction size was 5 ml, the first to four fractions were LMPs, and the fifth to ninth fractions were SMPs, and the last five fractions contain few particles.

Counting of TMPs

The concentration and size distribution of TMPs were measured by a Nanoparticle Tracking Analyzer (NTA, NanoSight Ltd.), which correlates the Brownian motion rate with the particle size. Each sample was diluted with sterile filtered PBS to three concentrations (10^6–10^8 pcs/ml). After the initial software optimization, the Brownian motion of each particle was tracked and measured. The two-dimensional Stokes–Einstein equation was used to calculate the particle size using the particle velocity. The NTA settings were optimized after the samples were collected and kept unchanged between samples, and then each video was analysed to give the average particle size, distribution and median of the particles, as well as the estimated concentration.

High-performance liquid chromatography (HPLC)

The concentration of MTX in MPs was measured by HPLC. MTX standards were purchased from Sigma-Aldrich. First, 200 µl of the sample was mixed with 600 µl of acetonitrile and chloroform mixture (acetonitrile:chloroform = 1:2), and then analysed on a C18 column (Nucleosil, 250 × 4.6 mm, Alltech) with an HPLC system (Thermo Fisher, UltiMate 3000). The mobile phase was composed of 10% acetonitrile and 0.01 mM KH2PO4 (ph 6.6). The flow rate was 1 ml/min, the column temperature was 30 ℃, and the MTX UV absorbance detection was performed at 304 nm.

Transmission electron microscopy

TMPs suspension with 20 µl was dropped onto the copper grid with carbon film for 3–5 min, and then the excess liquid was absorbed use by filter paper. TMPs were negatively stained with 2% phosphotungstic acid for 1–2 min, and dry at room temperature. The cuprum grids are observed and take images with a HT7800 electron microscope (HITACHI, Japan).

TMPs staining

TMPs were labelled with PKH-26 (Sigma-Aldrich) or near-infrared fluorescence DiR (Invitrogen) according to the instructions of the corresponding manufacturer. Briefly, the purified MPs were stained at 37 °C for 90 min after adding different fluorescent dyes (2 μl/ml PKH26 or 5 μM DiR). 2 ml 0.5% BSA/PBS was added to remove unbound dye, then the MPs were centrifuged at 4 °C at 14,000 x g for 60 min, and the pellet was washed twice with PBS. The MPs were resuspended in PBS for subsequent experiments.

Uptake of TMPs

In order to study the cell internalization of MPs, LLC cells and A549 cells were used as recipient cells. CFSE-labelled recipient cells were grown on 24-well plates and then incubated with PKH26-labelled MPs for different lengths of time. The cells were washed with PBS and fixed with 4% paraformaldehyde, and then the nuclei were stained with 4',6-diamidino-2-phenylindole dihydrochloride (DAPI). The cells were washed with PBS again and then imaged by a laser confocal scanning microscope (Nikon, C2-ER). The cells were incubated with PKH26-labeled MPs at 0, 2, 4, 6 h and resuspended in 400 μl PBS, and measured by flow cytometry to quantitatively evaluate cell uptake.

Distribution and metabolism of MPs in mice

MTX-MPs (100 μg MTX) or 100 μg MTX derived from 2.5×10^7 tumour cells were injected intravenously into LLC subcutaneous tumour mice to evaluate the tissue distribution of TMPs in vivo. Mice were killed at 0.5, 2, 4, 8, 12, and 24 h after injection, and heart, liver, spleen, lung, kidney and subcutaneous tumours were collected and weighed. HPLC was used to measure the amount of MTX in different tissues. 200 μg of organs or tissues were cut and ground into the slurry, and then 600 μl of cell lysis buffer was added and sonicated for 1 min. Next, the sample was treated with 800 μl of acetonitrile for 5 min, centrifuged at 14,000x*g* for 10 min, the supernatant was collected, and then 2 times the volume of chloroform was added and mix well, centrifuged at 14,000x*g* for 10 min and 200 μl of the aqueous phase was taken. The amount of MTX in different organs or tissues was detected by HPLC.

Animal tumour-bearing model and treatment

LLC or A549 cells were cultured in vitro to the logarithmic phase, and then harvested. Tumour cells (1×10^5 cells per mouse)were subcutaneously injected into the dorsal subcutaneous of C57BL/6 mice or BALB/c Nude mice, which was recorded as Day 0. The mice were randomly divided into 4 groups. From Day 7, PBS, MTX (10 μg), LMPs (contains 10 μg MTX) and SMPs (contains 10 μg MTX) were injected via tail vein once every other day, for a total of 6 times, and the tumour volume was measured every other day. On Day 22, 6 mice were dissected and the tumour weights were measured and the rest of the mice were kept for the study of long-term survival.

Flow cytometric analysis

To examine tumour-infiltrating T cells, tumour infiltrating leukocytes (TIL) were isolated and stained with antibodies against anti-mouse CD45 (clone 30-F11), CD3 (clone 145-2C11), CD4 (clone GK1.5), and CD8 (clone $53-6.7$). For intracellular cytokine staining, cells were treated with Fix/Perm solution and restained with anti-IFN-γ (clone XMG1.2) or anti-Granzyme B (clone GB11) antibody. For phenotypic analysis of DCs, cells were stained with surface antibodies: anti-CD11c (clone Bu15), anti-CD80 (clone 16-10A1), anti-CD86 (clone GL1). To examine the proliferation of T cells, CFSE-labelled T cells were incubated with activated DCs. All antibodies were purchased from Biolegend, and Flow cytometric analysis was performed with BD FACS Canto II.

Statistics analysis

All experiments were performed at least three times. Results were expressed as mean ± SEM and analysed by Student's t-test. The P-values < 0.05 were considered statistically significant. The analysis was conducted using the Graphpad 6.0 software.

Acknowledgements
We acknowledge Soundny (Sheng-Qi-An) Biotech (Wuhan, China) and the platform of Hubei Engineering Research Center of Tumour-Targeted Biochemotherapy for technical support on small animal in vivo imaging and two-photon laser scanning fluorescence microscope.

Author contributions
ZJ, KL, HL and JC conceived and designed the experiments. ZJ, KL, YL, BC, FM, HY, LZ, HY, WZ, TC, HY, QY, XW and SH performed the experiments. ZJ, KL, BC, HL and JC collected and analysed the data. HL and JC supervised the project. ZJ, KL, HL and JC wrote the manuscript. All authors reviewed the manuscript. All authors discussed the results and commented on the manuscript. All authors read and approved the final manuscript.

Funding
This study was supported by grants from Key Research and Develop Program of Hunan Province, China (Grant No. 2017WK2061), the Key R&D Program of Hubei Province (Grant No. 2020BCA068), Science and Technology Planning Project of Wuhan (Grant No. 2019020702011366).

Data availability
All data generated or analysed during this study are included in this published article.

Declarations

Ethics approval and consent to participate
All animal experiments were approved by the Institutional Animal Care and Use Committee at Xiangya School of Medicine, Central South University.

Consent for publication
Not applicable.

Competing interests
The authors declare no competing interests that might be perceived to influence the results and/or discussion reported in this paper.

Received: 12 January 2022 Accepted: 9 June 2022
Published online: 28 June 2022

References

Blanco E, Shen H, Ferrari M (2015) Principles of nanoparticle design for overcoming biological barriers to drug delivery. Nat Biotechnol 33(9):941–51
Gao Y, Zhang H, Zhou N, Xu P, Wang J et al (2020) Methotrexate-loaded tumour-cell-derived microvesicles can relieve biliary obstruction in patients with extrahepatic cholangiocarcinoma. Nat Biomed Eng. 4(7):743–753
Guo M, Wu F, Hu G, Chen L, Xu J et al (2019) Autologous tumor cell-derived microparticle-based targeted chemotherapy in lung cancer patients with malignant pleural effusion. Sci Transl Med. 11:474

Khani AT, Sharifzad F, Mardpour S, Hassan ZM, Ebrahimi M (2021) Tumor extracellular vesicles loaded with exogenous Let-7i and miR-142 can modulate both immune response and tumor microenvironment to initiate a powerful anti-tumor response. Cancer Lett. 501:200–209
Liang Q, Bie N, Yong T, Tang K, Shi X, Wei Z, Jia H, Zhang X, Zhao H, Huang W, Gan L, Huang B, Yang X (2019) The softness of tumour-cell-derived microparticles regulates their drug-delivery efficiency. Nat Biomed Eng. 3(9):729–740
Ma J, Zhang Y, Tang K, Zhang H et al (2016) Reversing drug resistance of soft tumor-repopulating cells by tumor cell-derived chemotherapeutic microparticles. Cell Res. 26(6):713–27
Mathieu M, Martin-Jaular L, Lavieu G, Théry C (2019) Specificities of secretion and uptake of exosomes and other extracellular vesicles for cell-to-cell communication. Nat Cell Biol 21(1):9–17
Mause SF, Weber C (2010) Microparticles: protagonists of a novel communication network for intercellular information exchange. Circ Res 107(9):1047–57
Moghimi SM (1995) Exploiting bone marrow microvascular structure for drug delivery and future therapies. Adv Drug Deliv Rev. 17:61–73
Moghimi SM (1995) Mechanisms of splenic clearance of blood cells and particles: towards development of new splenotropic agents. Adv Drug Deliv Rev 17:103–115
Ruihua M, Tiantian J, Degao C, Wenqian D, Huafeng Z et al (2016) Tumor cell-derived microparticles polarize M2 tumor-associated macrophages for tumor progression. Oncoimmunology. 5(4):1118599
Storm G, Belliot SO, Daemen T, Lasic DD (1995) Surface modification of nanoparticles to oppose uptake by the mononuclear phagocyte system. Adv Drug Deliv Rev 17:31–48
Tang K, Zhang Y, Zhang H, Xu P, Liu J et al (2012) Delivery of chemotherapeutic drugs in tumour cell-derived microparticles. Nat Commun 3:1282
Xu P, Tang K, Ma J et al (2020) Chemotherapeutic tumor microparticles elicit a neutrophil response targeting malignant pleural effusions. Cancer Immunol Res 8(9):1193–1205
Yanling S, Zheng Z, Zhang H, Yu Y, Ma Jingwei et al (2017) Chemotherapeutic tumor microparticles combining low-dose irradiation reprogram tumor-promoting macrophages through a tumor-repopulating cell-curtailing pathway. Oncoimmunology 31(6):e1309487
Yuana Yuana A, Sturk Y, Nieuwland R, Rienk (2013) Extracellular vesicles in physiological and pathological conditions. Blood Rev 27(1):31–39
Zhang H, Tang K, Zhang Y, Ma R, Ma J et al (2015) Cell-free tumor microparticle vaccines stimulate dendritic cells via cGAS/STING Signaling. Cancer Immunol Res 3(2):196–205

Publisher's Note